NRC·CNRC

NRC Publications Archive
Archives des publications du CNRC

Agarose/crystalline nanocellulose (CNC) composites promote bone marrow-derived mast cell integrity, degranulation and receptor expression but inhibit production of de novo synthesized mediators

Kulka, Marianna; Wagner, Ashley; Cho, Jae-Young; Alam, Syed Benazir; Santos, Joy Ramielle; Jovel, Juan; Karamchand, Leshern; Marcet-Palacios, Marcelo

This publication could be one of several versions: author's original, accepted manuscript or the publisher's version. / La version de cette publication peut être l'une des suivantes : la version prépublication de l'auteur, la version acceptée du manuscrit ou la version de l'éditeur.
For the publisher's version, please access the DOI link below./ Pour consulter la version de l'éditeur, utilisez le lien DOI ci-dessous.

Publisher's version / Version de l'éditeur:
https://doi.org/10.3389/fbioe.2023.1160460
Frontiers in Bioengineering and Biotechnology, 11, 2023-04-11

NRC Publications Archive Record / Notice des Archives des publications du CNRC :
https://nrc-publications.canada.ca/eng/view/object/?id=6aac7d91-f396-4df4-a05d-06b7ef6aad94
https://publications-cnrc.canada.ca/fra/voir/objet/?id=6aac7d91-f396-4df4-a05d-06b7ef6aad94

Access and use of this website and the material on it are subject to the Terms and Conditions set forth at
https://nrc-publications.canada.ca/eng/copyright
READ THESE TERMS AND CONDITIONS CAREFULLY BEFORE USING THIS WEBSITE.

L'accès à ce site Web et l'utilisation de son contenu sont assujettis aux conditions présentées dans le site
https://publications-cnrc.canada.ca/fra/droits
LISEZ CES CONDITIONS ATTENTIVEMENT AVANT D'UTILISER CE SITE WEB.

Questions? Contact the NRC Publications Archive team at PublicationsArchive-ArchivesPublications@nrc-cnrc.gc.ca. If you wish to email the authors directly, please see the first page of the publication for their contact information.

Vous avez des questions? Nous pouvons vous aider. Pour communiquer directement avec un auteur, consultez la première page de la revue dans laquelle son article a été publié afin de trouver ses coordonnées. Si vous n'arrivez pas à les repérer, communiquez avec nous à PublicationsArchive-ArchivesPublications@nrc-cnrc.gc.ca.

National Research Council Canada | Conseil national de recherches Canada

Canada

frontiers | Frontiers in Bioengineering and Biotechnology

TYPE Original Research
PUBLISHED 11 April 2023
DOI 10.3389/fbioe.2023.1160460

Check for updates

OPEN ACCESS

EDITED BY
Dorela Doris Shuboni-Mulligan,
Eastern Virginia Medical School,
United States

REVIEWED BY
Aurelia Drzewiecka,
Polish Academy of Sciences, Poland
Rebecca Kelley Martin,
Virginia Commonwealth University,
United States

*CORRESPONDENCE
Marianna Kulka,
marianna.kulka@nrc-cnrc.gc.ca

SPECIALTY SECTION
This article was submitted to Biomaterials, a section of the journal Frontiers in Bioengineering and Biotechnology

RECEIVED 07 February 2023
ACCEPTED 22 March 2023
PUBLISHED 11 April 2023

CITATION
Kulka M, Wagner A, Cho J-Y, Alam SB, Santos JR, Jovel J, Karamchand L and Marcet-Palacios M (2023), Agarose/crystalline nanocellulose (CNC) composites promote bone marrow-derived mast cell integrity, degranulation and receptor expression but inhibit production of *de novo* synthesized mediators.
Front. Bioeng. Biotechnol. 11:1160460.
doi: 10.3389/fbioe.2023.1160460

COPYRIGHT
© 2023 Kulka, Wagner, Cho, Alam, Santos, Jovel, Karamchand and Marcet-Palacios. This is an open-access article distributed under the terms of the Creative Commons Attribution License (CC BY). The use, distribution or reproduction in other forums is permitted, provided the original author(s) and the copyright owner(s) are credited and that the original publication in this journal is cited, in accordance with accepted academic practice. No use, distribution or reproduction is permitted which does not comply with these terms.

Agarose/crystalline nanocellulose (CNC) composites promote bone marrow-derived mast cell integrity, degranulation and receptor expression but inhibit production of *de novo* synthesized mediators

Marianna Kulka[1,2]*, Ashley Wagner[1], Jae-Young Cho[1], Syed Benazir Alam[1], Joy Ramielle Santos[3], Juan Jovel[4], Leshern Karamchand[1] and Marcelo Marcet-Palacios[5]

[1]Nanotechnology Research Centre, National Research Council Canada, Edmonton, AB, Canada, [2]Department of Medical Microbiology and Immunology 6-020 Katz Group Centre, University of Alberta, Edmonton, AB, Canada, [3]Department of Medicine, University of Alberta, Edmonton, AB, Canada, [4]The Metabolomics Innovation Centre (TMIC), 7-12 Heritage Medical Research Centre, University of Alberta, Edmonton, AB, Canada, [5]Northern Alberta Institute of Technology, Edmonton, AB, Canada

Introduction: Mast cells are highly granulated tissue-resident leukocytes that require a three-dimensional matrix to differentiate and mediate immune responses. However, almost all cultured mast cells rely on two-dimensional suspension or adherent cell culture systems, which do not adequately reflect the complex structure that these cells require for optimal function.

Methods: Crystalline nanocellulose (CNC), consisting of rod-like crystals 4–15 nm in diameter and 0.2–1 μm in length, were dispersed in an agarose matrix (12.5% w/v), and bone marrow derived mouse mast cells (BMMC) were cultured on the agarose/CNC composite. BMMC were activated with the calcium ionophore A23187 or immunoglobulin E (IgE) and antigen (Ag) to crosslink high affinity IgE receptors (FcεRI).

Results: BMMC cultured on a CNC/agarose matrix remained viable and metabolically active as measured by reduction of sodium 3′-[1-[(phenylamino)-carbony]-3,4-tetrazolium]-bis(4-methoxy-6-nitro) benzene-sulfonic acid hydrate (XTT), and the cells maintained their membrane integrity as analyzed by measuring the release of lactate dehydrogenase (LDH) and propidium iodide exclusion by flow cytometry. Culture on CNC/agarose matrix had no effect on BMMC degranulation in response to IgE/Ag or A23187. However, culture of BMMC on a CNC/agarose matrix inhibited A23187-and IgE/Ag-activated production of tumor necrosis factor (TNF) and other mediators such as IL-1β, IL-4, IL-6, IL-13, MCP-1/CCL2, MMP-9 and RANTES by as much as 95%. RNAseq analysis indicated that BMMC expressed a unique and balanced transcriptome when cultured on CNC/agarose.

Discussion: These data demonstrate that culture of BMMCs on a CNC/agarose matrix promotes cell integrity, maintains expression of surface biomarkers such as

FcεRI and KIT and preserves the ability of BMMC to release pre-stored mediators in response to IgE/Ag and A23187. However, culture of BMMC on CNC/agarose matrix inhibits BMMC production of *de novo* synthesized mediators, suggesting that CNC may be altering specific phenotypic characteristics of these cells that are associated with late phase inflammatory responses.

KEYWORDS

mast cell, nanocellulose, cytokines, inflammation, IgE

Introduction

Most cell culture methods rely on two-dimensional (2D) arrangements where cells are grown either in a single monolayer on a plastic (i.e., polystyrene) surface or in suspension in liquid media. In tissues, however, most cells function within a complex three-dimensional (3D) microenvironment and interact with a protein-rich extracellular matrix and nearby cells in a spatially coordinated manner. For this reason, 3D culture scaffolds have become increasingly popular, particularly polymer-based structures that enable cells to grow upon or within them. In order for such a 3D matrix to be compatible with cell culture it must maintain a stable structure but should not interfere with normal cellular processes (also referred to as "biologically inert"). In some cases, the matrix can be biocompatible such that it facilitates or promotes normal cellular functions such as differentiation, division, chemotaxis and secretion. To be biocompatible, a matrix must have appropriate osmolarity and pH. Importantly, to enable nutrient and gas exchange the materials must also have adequate porosity.

Cellulose polymers have been used to culture stem cells and progenitor cell colonies because they maintain their structure and are generally considered to be biologically inert. Some of the earliest hemopoietic stem cell cultures were performed using methylcellulose media since this allowed for removal of individual colonies using micromanipulators (Ogawa et al., 1984) and promoted a more mature phenotype (Kurosawa, 2007). In particular, tissue-resident immune cells such as mast cells were cultured in such gel-based 3D structures for decades (Nakahata et al., 1982; Denburg et al., 1983) which allowed for manipulation of their differentiation pathways and analysis of their interactions with other cell types (Bienenstock et al., 1987; Kurosawa, 2007). Despite the importance of these semi-solid gel-based culture techniques in cell culture, there has been very little advancement in semi-solid culture substrates. Furthermore, the effect of the semi-solid media on cell function and viability has been seldom examined.

Crystalline nanocellulose (CNC) hydrogels are a novel and versatile culture substrate for cell culture because they are porous and can be chemically modified with functional groups or embedded with cell-specific biomolecules (Ma et al., 2022). Nanocellulose in the crystalline form has distinct effects on cell viability and function (Mortensen et al., 2022) and can be complexed with proteins such as casein to form composites or coupled with lysine molecules to promote cell proliferation and differentiation (Pandanaboina et al., 2021; Biranje et al., 2022). Much of the recent work with nanocellulose has relied on bacterial sources since it is low cost and easy to produce (Ugrin et al., 2021), but the presence of endotoxin in such preparations, especially when culturing immune cells, remains a concern (Moriyama et al., 2022).

In this study, we used plant-based nanocellulose crystals to assemble a CNC/agarose hydrogel matrix and determined its suitability for the culture of mouse bone marrow-derived mast cells (BMMC). Mast cells are a tissue-resident leukocyte that is absent from blood and therefore exclusively differentiates and functions in a 3D tissue environment. BMMC are not a transformed cell line and as such they exhibit aberrant growth and differentiation. BMMC are derived from wild type bone marrow stem cells and therefore are expected to respond to a 3D matrix environment like their *in vivo* counterparts. In this study, we examined the behaviour of BMMC activated with immunoglobulin E (IgE) and antigen (Ag) to crosslink high affinity IgE receptors (FcεRI) that is a classic stimulus of allergic inflammation. These responses were compared to activation using a receptor-independent stimulus (calcium ionophore A23187) which circumvents the cell membrane-proximal signaling associated with inflammatory stimuli. In both cases, BMMC production of several mediators including tumor necrosis factor alpha (TNF), a potent pro-inflammatory cytokine, was measured. The effect of the CNC/agarose matrix on cell viability was measured using three independent analyses of cell health, including measurement of NADH-dependent XTT reduction, propidium iodide (PI) incorporation, and lactate dehydrogenase (LDH) release. The expression of surface biomarkers such as the high affinity IgE receptor (FcεRI) and the stem cell factor receptor KIT/CD117 was determined using flow cytometry. Changes in mast cell transcriptome when cultured on CNC/agarose was analyzed using RNA sequencing (RNAseq).

Materials and methods

Materials and reagents

Spray dried crystalline nanocellulose (CNC) were kindly provided by Innotech Alberta (batch no. Comp181121-H). Agarose powder was purchased from Thermo Scientific (electrophoresis grade). All other reagents were prepared or purchased as indicated.

Fabrication and characterization of the CNC/agarose substrate

For the transmission electron microscopy (TEM) studies, 0.02 wt% aqueous CNC solution was prepared by sonication for 10 s and deposited on a carbon-coated 400-mesh copper TEM grid (Electron Microscopy Sciences; CF400-Cu), and the excess solution was blotted after 10 s. Staining for TEM was performed by

depositing one droplet of 2% uranyl acetate (UA) solution, then after 120 s, blotting and drying in air. TEM investigation was carried out on a JEOL 2200FS TEM—200 kV Schottky field emission instrument equipped with an in-column omega filter. Bright field TEM images were acquired using energy filtered zero loss beams (slit width 10 eV).

For atomic force microscopy (AFM), a clean silicon wafer substrate (1 cm^2 × 1 cm^2) was prepared and pre-treated with poly-L-lysine: 5 µL of an aqueous poly-L-lysine solution were deposited on a clean silicon wafer substrate (1 cm^2 × 1 cm^2) and incubated for 30 s, after which the sample surface was rinsed with DI water. Then, this silicon substrate was spin-coated with 0.02 wt% CNC solution at 2,500 rpm, and dried in air for 1 day. Surface morphology of CNC particles was characterized using a Veeco Dimension 3100 AFM. For optimized image quality, high resolution, soft tapping mode AFM probes (MikroMasch United States, Inc.) with low spring constants of 5.0 N/m and 1 nm radii were used.

For the cryo-scanning electron microscopy (cryo-SEM) imaging, each gel sample was placed on a small copper-based rivet, and a second rivet was carefully placed above. Then, the two-rivet ensemble was frozen by plunging vertically into liquid nitrogen (LN_2). The frozen ensemble samples were then fractured to reveal the internal structure of or without the agarose/CNC composite. The revealed fracture surface was then sublimated for 30 min at −100°C and subsequently sputter-coated with Pt in a cryo-coater (Leica ACE600). After this, the sample was transferred to a cryo-stage SEM (Zeiss NVision40) with temperature controller and observed under an accelerating voltage of 3 keV at −100°C using the in-lens EsB (energy and angle selective backscattered electron) detector.

Generation of the BMMC

C57BL/6 mice were sacrificed between 6 and 10 weeks old and bone marrow from their femurs was obtained by aspiration in accordance with the University of Alberta Animal Care Committee approved standard protocols and procedures. Aspirates were maintained in RPMI-1640 media (Gibco, Burlington, ON, Canada) supplemented with 4 mM L-glutamine (Gibco), 50 µM BME (Sigma-Aldrich, Oakville, ON, Canada), 1 mM sodium pyruvate (Gibco), 100 U/mL penicillin/100 µg/mL streptomycin (Gibco), 0.1 mM non-essential amino acids (Gibco), 25 mM HEPES (Gibco), 10% FBS (Gibco) and 30 ng/mL mouse recombinant IL-3 (Peprotech, Rocky Hill, NJ, United States), henceforth referred to as complete-RPMI. Cells were fed every 3–5 days. After 4 weeks, cell purity was determined by measuring expression of CD117 (KIT) and FcεRI by flow cytometry. After 4 weeks, 99% of cells were double positive for KIT and FcεRI.

Generation of the CNC/agarose matrix and cell culture

Agarose powder was added to phosphate buffered saline (PBS) without magnesium or calcium (Gibco; 2% w/v) and heated to 100°C, while CNC powder was dissolved in PBS (2%–25% w/v), heated to 37°C for 5 min and mixed 1:1 with hot 2% agarose. Immediately after heating, 50 or 500 µL of the solution was added to the wells of a 96-well or 24-well culture plate (Thermo Fisher, Waltham, United States) respectively, and left at room temperature for 30 min to set.

For CNC/agarose composites supplemented with complete-RPMI, CNC powder was dissolved in complete-RPMI (25%), the mixture was heated to 37°C for 5 min, and mixed 1:1 with a hot 2% agarose solution prepared in complete-RPMI. The hot CNC/agarose + complete-RPMI mixture was added to the wells of a 24-well culture plate and left at room temperature for 30 min to set. BMMC were grown in complete-RPMI on top of the CNC/agarose composites (Supplementary Figure S1).

Analysis of cell metabolic activity by measuring activity of NADH

BMMC were cultured on CNC/agarose composites (or standard untreated cell culture wells as controls) in a 96-well plate, at a density of 5,000 cells/well for 24 h at 37°C and a humidified atmosphere with 5% CO_2. After treatment, 50 µL of XTT (sodium 3′-[1-[(phenylamino)-carbony]-3,4-tetrazolium]-bis(4-methoxy-6-nitro) benzene-sulfonic acid hydrate) with electron coupling reagent (Roche, Basel, Switzerland) was added to the wells and incubated in a humidified atmosphere at 37°C with 5% CO_2 for 24 h to allow formation of soluble formazan salt. One hundred mL was aspirated from each well, transferred to a fresh 96-well plate and absorption was measured at 450 nm with a reference wavelength of 660 nm using a Varioskan Lux microplate reader (Thermo Fisher).

Colorimetric analysis of LDH release

BMMC were sensitized with 500 ng/mL mouse anti-DNP IgE (SPE-7, Sigma) for 16 h or cultured in fresh media without IgE (unsensitized). The BMMC were washed with fresh media and placed onto the CNC/agarose composites (or standard untreated cell culture wells as controls) at a density of 15,000 cells/well and IgE sensitized cells were stimulated with 10 ng/mL DNP-BSA (Invitrogen) and unsensitized cells were stimulated with 1 µM A23187 for 18 h in a humidified atmosphere at 37°C with 5% CO_2. After treatment, the cells were spun at 200 rcf (× *g*) for 5 min, and 50 µL of the supernatants were collected and aliquoted into a fresh 96-well plate. For total LDH wells, 50 µL of 0.1% Triton (Fisher, Hampton, NH, United States) was added to lyse the cells. Fifty µL of the LDH assay reagent (iodonitrotetrazolium dinucleotide sodium salt (4 mM), β-nicotinamide adenine dinucleotide sodium salt (6.44 mM), lithium L-lactate (320 mM), and TrisBase [2-amino-2-(hydroxymethyl)-1,3-propanediol (pH 8.2, 0.2 M)] was added to the wells and left to incubate in the dark at room temperature for 90 min. To stop the reaction, 50 µL of acetic acid (1 M) was added to the wells, and the absorption was measured using a Varioskan Lux microplate reader (ThermoFisher) at 490 nm with a reference wavelength of 680 nm.

Propidium iodide exclusion assay of membrane integrity

BMMC were cultured on CNC/agarose hydrogel matrix for 18 or 24 h. Cells were removed carefully and washed twice with phosphate-buffered saline (PBS)-0.5% w/v bovine serum albumin (BSA) (Sigma-Aldrich) at 300 × *g* for 5 min at room temperature followed by resuspension in PBS-0.5% BSA at a final density of 1.5×10^6 cells/mL. Cells were treated with 10 µg/mL propidium iodide (Invitrogen) for 1 h at 4°C in the dark. Fluorescence data was acquired using a CytoFlex flow cytometer (Beckman Coulter, Brea, CA, United States) equipped with an Argon ion laser (488–514 nm) and bandpass filter to enable detection fluorescence emission at 578 nm. 20,000 events at a flow rate of 30 µL/min was acquired for each sample at room temperature. As mast cells are highly granular (high side scatter, SSC) and large in size (high forward scatter, FSC) when compared to other immune cell types, such as monocytes and lymphocytes, a well-defined cell population containing relatively high FSC and SSC were gated and analyzed. This also served to preclude the cell debris with low FSC and SSC values. Data was generated using FlowJo 10.6.2 software (Becton, Dickinson and Company, Ashland, OR, United States).

Analysis of FcεRI and KIT expression

BMMC were washed with PBS containing 0.5% BSA (Sigma) re-suspended in PBS containing 0.5% BSA (1.5×10^6 cells/mL), and then incubated with 6 ng/mL rat anti-mouse CD117(KIT)-PE (eBioscience, San Diego, CA, United States) and 6 ng/mL Armenian hamster anti-mouse FcεRI-APC (eBioscience) for 1 h at 4°C. After washing with 0.5% BSA in PBS twice, cells were re-suspended in 100 µL 0.5% BSA/0.05% sodium azide in PBS and transferred to a round bottom 96-well plate. Cell samples were analyzed on a CytoFlex flow cytometer (Beckman Coulter, Brea, CA, United States). Rat IgG2b K -PE (eBioscience) and Armenian hamster IgG - APC (eBioscience) were used as isotype controls. Data was generated using FlowJo 10.6.2 software (Becton, Dickinson and Company, Ashland, OR, United States).

RNA isolation and RNAseq analysis of BMMC transcriptome

BMMC were cultured on 12.5% CNC/agarose or agarose alone (2% (w/v) in PBS)) (three technical replicates each) at a density of 1×10^6 cells/mL for 6 h and recovered from the composites by gentle aspiration. Total RNA was extracted from each of the technical replicates using TriZol (Invitrogen) and RNeasy columns (Qiagen, Hilden, Germany). On-column digestion of contaminating DNA was performed with DNase I prior to elution of RNA from the columns. Total RNA integrity was subsequently assessed using an Agilent Technologies 2,100 Bioanalyzer and each RNA isolate was confirmed to have an RNA Integrity Number (RIN) value > 9.0 (Supplementary Information). Thereafter, the mRNA in each total RNA isolate was converted into cDNA libraries and enriched *via* PCR using the Illumina TruSeq RNA Sample Preparation kit v2 (San Diego, CA, United States). The cDNA libraries (3x CNC/agarose and 3x agarose alone) were subsequently sequenced using the Illumina MiSeq Reagent kit v3 (San Diego, CA, United States).

RNAseq libraries were constructed from 100 ng of total RNA, using the TrueSeq RNA library prep kit v2 (Illumina). In brief, polyadenylated mRNAs were enriched using oligo dTs conjugated to paramagnetic beads. Enriched mRNA was chemically fragmented and reverse transcribed into cDNA. cDNAs were end-repaired, A-tailed, ligated to add adapters and finally indexed through PCR. Libraries were sequenced on a MiSeq instrument using a 75-cycle protocol that included in-instrument demultiplexing of samples. Raw sequences were inspected for quality, and no trimming was required because Q scores were on average close to 30. Sequences were pseudo-aligned against the mouse transcriptome (GRCm39) using Kallisto, with 100 bootstraps and bias correction (Bray et al., 2016a; Bray et al., 2016b). Count data were then analyzed with DESeq2 (Love et al., 2014). Briefly, RNAseq counts were modeled using a negative binomial distribution, and differential expression of transcripts were evaluated with the Ward test. *p* values were corrected with the Benjamini–Hochberg method and comparisons with corrected pValues <0.05 were considered significant.

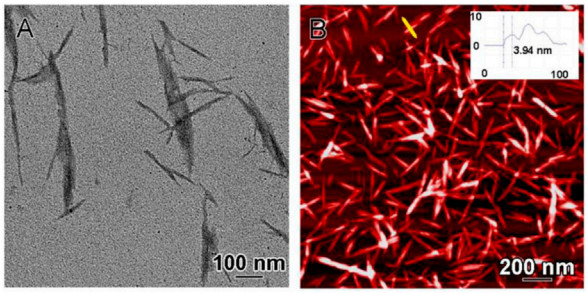

FIGURE 1
CNC morphologic and dimensional characterization. **(A)** Characterization of CNC by TEM and **(B)** AFM: inset shows the cross-sectional height profile along the yellow line which suggests multi-layered stacking of CNC—the thickness (height) of single layer is around 4 nm and the width is approximately 6 nm (inset).

TNF analysis by ELISA and electrochemiluminescent multiplex analysis

BMMC were seeded at a density of 1×10^6 cells/mL onto the CNC/agarose composites or standard untreated cell culture plates as controls and incubated for 18 h. BMMC were then washed and sensitized with 500 ng/mL mouse anti-DNP IgE (SPE-7, Sigma) or cultured in fresh media without IgE (unsensitized control) for 18 h. BMMC were then stimulated with either 10 ng/mL DNP-BSA (Invitrogen) or 1 µM A23187 for 18 h at 37°C. Following activation, cell suspensions were centrifuged at 200 *g* × for 5 min

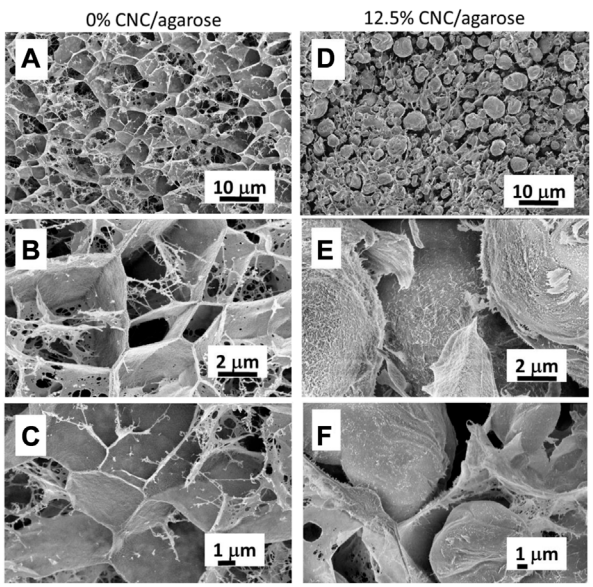

FIGURE 2
CNC/agarose and agarose gel characterization. Characterization of 1% Agarose gel without CNC (0%) **(A–C)** or with CNC (12.5%) **(D–F)** by cryo-SEM at various resolutions.

and cell-free supernatants were collected. Supernatants were analysed *via* commercial ELISA (ThermoFisher) and Meso Scale multiplex assays (Meso Scale Discovery, Rockville, MD, United States) following manufacturer instructions, and plates were read using the Varioskan Lux (ThermoFisher) and MESO QuickPlex SQ 120 MM (Meso Scale Discovery) plate readers respectively.

Statistical analysis

Experiments were conducted in triplicate or quadruplicate and values represent the mean of 3 biological replicates ±standard deviation of the mean. *p*-values were determined by one-way ANOVA (between groups) with appropriate post-hoc analysis or Student t-tests.

Results

Preparation of the CNC/agarose matrix for cell culture analysis and effect on cell viability

The CNC used for this study was obtained as a powder and characterized using TEM and AFM (Figures 1A, B). By TEM (Figure 1A) the CNC appeared as long rod-shaped, spindle-like structures approximately 6 nm wide and 200 nm long, with an electron dense outer surface. The CNC nanorods appear as multilayered structures (see AFM data in Figure 1B), possibly through aggregation/stacking of multiple constituent CNC elements.

The structures of agarose and CNC/agarose gels were characterized by cryo-SEM. The agarose gel was an ordered, porous honey-comb matrix composed of polyhedral chambers with flat faces (Figures 2A–C). The characteristic dimensions of each chamber are in the 2-5 µm range, although some anisotropy is often noted along one axis. The interiors of the chambers were mainly empty, but some chambers had fibrils attached to the walls and spanning the entire chamber almost like a scaffold.

The addition of CNC significantly altered the morphology of the gel from angular structures, to spherical, ball-like structures (Figures 2D–F). The spherical structures varies in size from less than 1 µm to approximately 5 µm, and they were arranged within complex fibril-like composites (Figure 2D). Each ball-like structure has a rather smooth surface that appears increasingly fibrous with increasing magnification (Figure 2E), and these fibres are likely rich in the CNC component. The ball structures are interspersed with thin membrane-like sheets (Figure 2F).

The CNC/agarose matrix incorporated 12.5% (w/v) CNC. BMMC were cultured on the surface of the CNC/agarose matrix or on agarose alone for 18 h, and the size and granularity of the cell population was analyzed by flow cytometry (Figures 3A, B). Cells cultured on the agarose or CNC/agarose composites formed a normally distributed population of large and granular cells as measured by flow cytometry, similar to our previous studies (Karamchand et al., 2021; Alam et al., 2022). To determine the effect of the CNC/agarose composites on cell viability, BMMC were washed with PBS and then exposed to propidium iodide, a DNA chelating dye that fluoresces when bound to DNA (Benassi et al., 2022; Jin et al., 2022). When cells undergo necrosis or are in the later stages of apoptosis, their membrane integrities are severely compromised, and they fluoresce when exposed to propidium iodide. This effect has been routinely used as a measure of cell permeability and viability (Samarghandian et al., 2019). Flow cytometric analysis of BMMC indicated that the CNC/agarose matrix had no detectable effect on cell membrane integrity (Figures 3C, D), suggesting that the cells were healthy and their cell membranes were intact and undamaged.

Microenvironmental stress can cause metabolic changes that result in the release of intracellular enzymes such as LDH (Gabr et al., 2022). BMMC were cultured on CNC/agarose, and LDH release was measured using a standard approach as described in the materials and methods. Surprisingly, culture of BMMC on CNC/agarose resulted in a decrease in LDH release compared to cells grown in the cell culture plate alone, indicating that the CNC/agarose matrix was, in fact, promoting cell integrity (Figure 3E).

Mast cell activation can be influenced by changes in metabolic rate (Matsumura et al., 2022). To determine whether CNC/agarose composites can modify the metabolic rate of BMMC, the activity of mitochondrial NADH was assessed. When BMMC were cultured on CNC/agarose, their metabolic rate decreased by 15% (Figure 3F) compared to cells that were cultured on agarose alone.

The CNC/agarose matrix does not change BMMC expression of FcεRI and KIT

Two of the most important biomarkers of BMMC function and differentiation are FcεRI and KIT (CD117), the receptors for

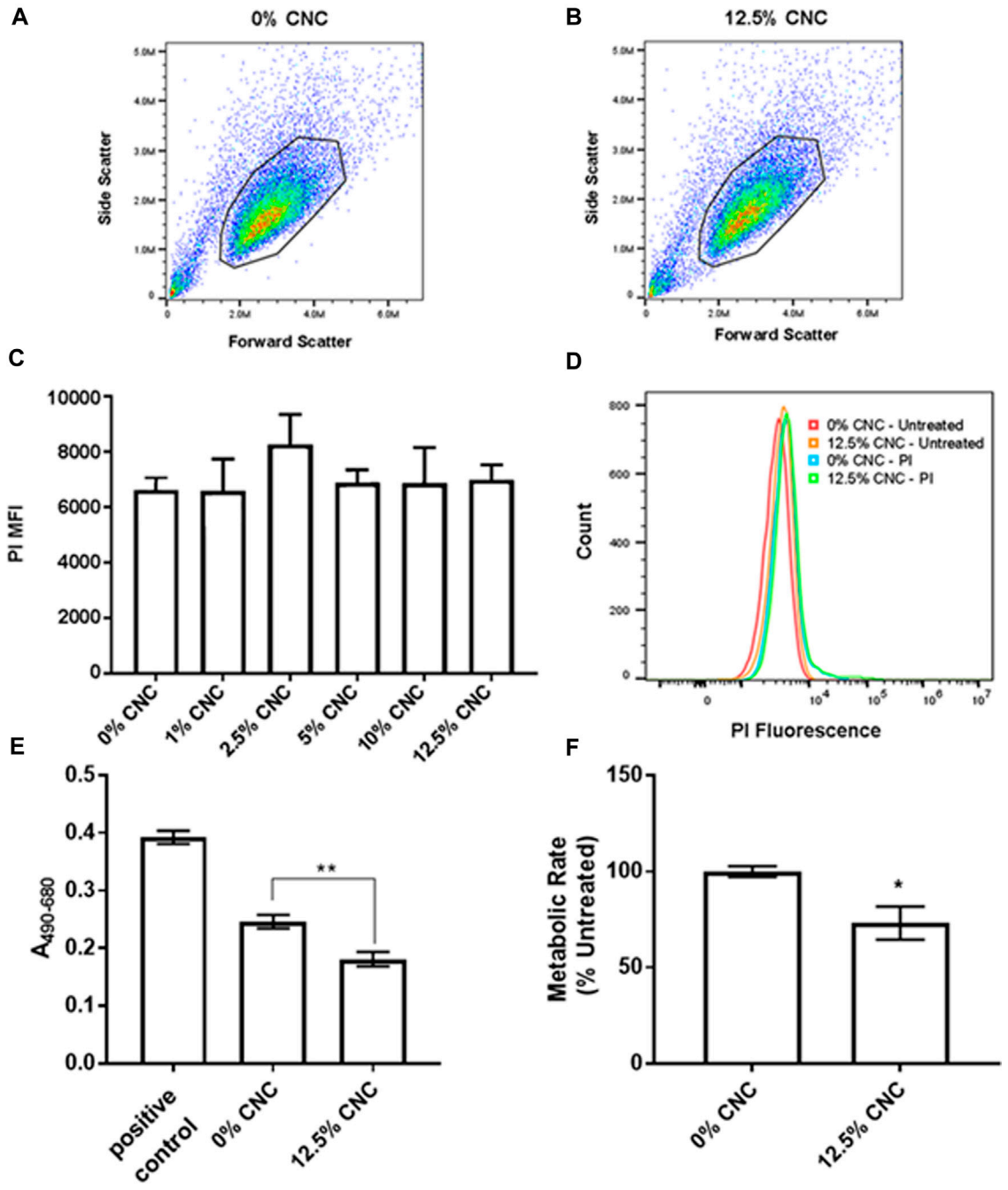

FIGURE 3
Viability and metabolic activity of cells cultured on CNC/agarose substrates. **(A, B)** Forward scatter (*X*-axis) versus side scatter (*Y*-axis) dot plot analysis of total cell population from **(A)** untreated control BMMC (0% CNC) and **(B)** BMMC cultured on 12.5% CNC/agarose substrate for 18 h depicting the gated cell population used for data analysis. **(C)** BMMCs were cultured on different CNC/agarose substrate concentrations (1%–12.5% (w/v) CNC) for 18 h, and cell membrane integrity was determined by flow cytometric analysis of propidium iodide (P1) stained cells. Graphical representation of PI mean fluorescence intensity (MFI) for BMMCs incubated on different CNC/agarose substrates relative to BMMCs that were untreated (0% CNC/agarose) and stained with PI (n = 4). **(D)** Histogram overlay profile of gated cells (unstained or stained with PI), from untreated control BMMCs (0% CNC/agarose) and BMMCs cultured on 12.5% CNC/agarose. **(E)** LDH release from BMMC incubated on CNC/agarose matrix for 24 h with a 0.1% triton X-100 positive control for LDH release. **(F)** BMMC were incubated on CNC/agarose matrix for 24 h and metabolic activity was determined by measuring reduction of XTT. **(E, F)** Statistical analysis used was One-Way ANOVA with Dunnett's post-hoc test or Student T-test relative to 0% CNC, p 0.05 (*), p S 0.01 (**). Experiments were performed in triplicate and biological replicate of n-3.

immunoglobulin E (IgE) and stem cell factor which are important for mast cell differentiation, longevity and function (Matsumura et al., 2022). When BMMC are maintained in culture, their expression of FcεRI and KIT can change over time (Matsumura et al., 2022), and changes in expression in either of these biomarkers signals undesirable changes in BMMC phenotype.

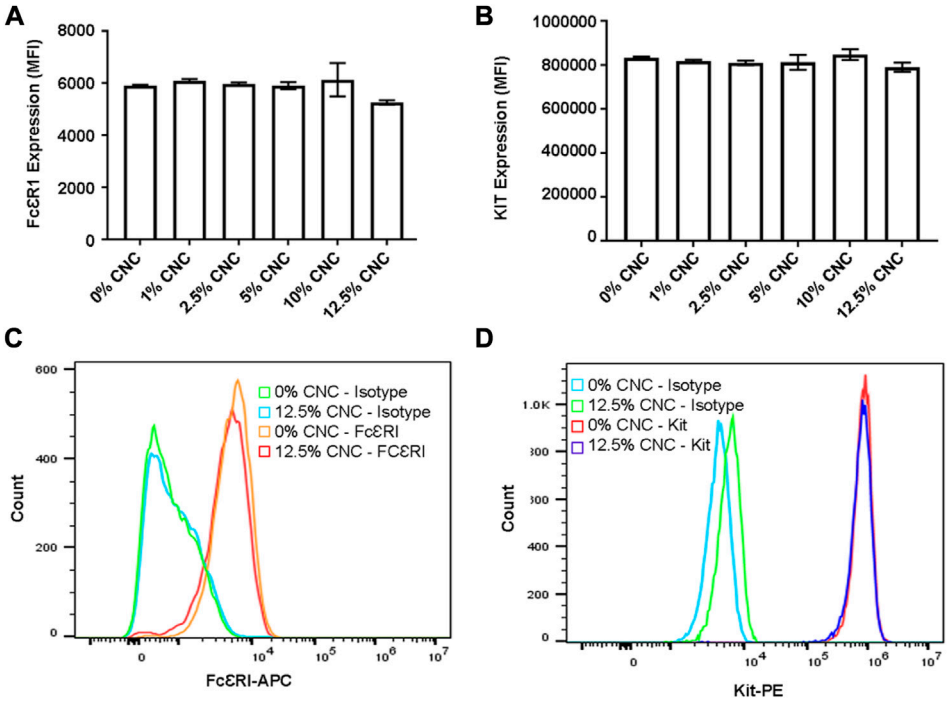

FIGURE 4
Flow cy-toinctric analysis of FceRI and Kit (0117) cell surface receptor expression post incubation on CNC/agarose substrates. BMMCs were cultured either in the absence or presence of CNC/agarose substrates (0%–12.5%) for 18 h and analyzed for FecR1 and Kit receptor expression *via* flow cytometry. Graphical representation of MFIs of untreated BMMCs (0% CNC) or BMMC incubated with 12.5% CNC/agarose substrates labeled with **(A)** anti-FccRI-APC or **(B)** anti-KIT-PE antibodies. **(C)** Histogram overlay profile of untreated BMMCs (0% CNC) or BMMC incubated with 12.5% CNC/agarose substrates and stained with anti-FccRI-APC antibody or its isotype control. **(D)** Histogram overlay profile of BMMCs incubated either alone (0% CNC) or with 12.5% CNC/agarose substrates and stained with anti-Kit-PE antibody or its isotype control. Experiments were performed with biological replicate of $n = 4$.

When BMMC were cultured on the CNC/agarose matrix for 18 h, there were no discernable effects on the expression of FcεRI or KIT as measured by flow cytometry (Figures 4A, B) even at the highest concentration of CNC (12.5%). Although there was a slight decrease in FcεRI expression when the BMMC were cultured on the 12.5% CNC, this slight decrease was not statistically significant. A representative histogram overlay of FcεRI and KIT expression (Figures 4C, D) confirms that there were no detectable changes in either FcεRI or KIT expression, suggesting that the cells' phenotype remains stable when they are cultured on the CNC composites.

CNC/agarose can be supplemented to support various culture requirements

To determine whether the 3D culture system modulates the expression of FcεRI and KIT and viability/cell membrane integrity compared to conventional 2D liquid culture, we constructed a CNC/agarose hydrogel prepared in complete RPMI in place of PBS. This matrix contains all the required nutrients, including supplements such as FBS and IL-3, which are required for optimal BMMC growth. BMMC grown on the CNC/agarose + complete-RPMI hydrogel resulted in relatively normal expression of FcεRI and KIT (Figure 5A) and no significant change in viability/cell membrane integrity as measured by propidium iodide staining (Figures 5B, C) when compared to BMMC cultured in liquid with complete RPMI alone.

The CNC/agarose matrix modifies BMMC transcriptome

To determine the effect of culturing the BMMC on a CNC matrix, we isolated RNA from BMMC cultured on the matrix for 6 h and examined gene expression using RNAseq (Figure 6). Principle component analysis demonstrated that the CNC/agarose replicates clustered separately from the agarose-only replicates, suggesting that culturing of BMMC on the CNC/agarose substrate significantly altered the BMMC transcriptome relative to the control (agarose only). Genes in the CNC/agarose treatment were considered to be significantly differentially expressed if they exhibited a $\log_2$ fold change value of ± 1 relative to the control.

This analysis revealed that more than 1000 genes were regulated by culturing the cells on CNC/agarose compared to agarose alone (Figure 6A). A volcano analysis indicates that more than 500 genes were upregulated and more than 200 genes were downregulated. TNF signalling pathway genes, such as *Birc3, Fadd, Lif, Mapk14, Ccl2* and *Fos*, were consistently downregulated as shown in red (Figure 6A). To better understand the possible associations between these genes, we analyzed functional links between them using the search tool for the retrieval of interacting genes/proteins (STRING) database. STRING

10.3389/fbioe.2023.1160460

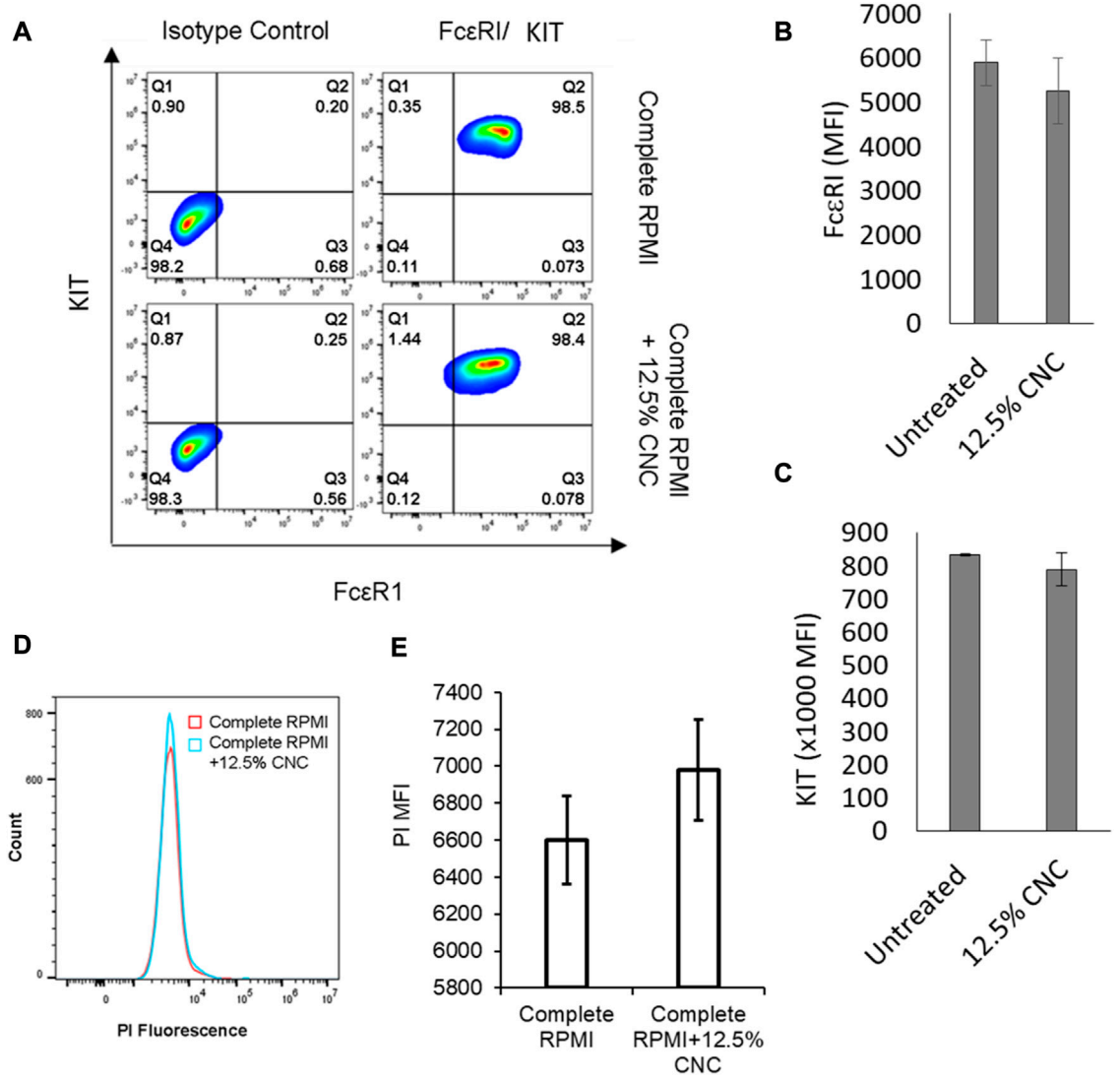

FIGURE 5
Effect of CNC/agarose substrates supplemented with complete RPMI on phenotypic expression and plasma membrane integrity of BMMC. **(A)** BMMCs were cultured in absence (Complete RPMI) or presence (Complete RPMI +12.5% CNC) of CNC/agarose substrates for 24 h. Cells were removed and analyzed for receptor expression by labeling with either the isotype controls or antibodies. KIT (*Y*-axis) versus FcsRI (*X*-axis) expression contour plots are representative of 3 independent experiments. BMMC were cultured on 0%–12.5% CNC/agarose as in **(A)** and expression of FcsRI **(B)** and KIT **(C)** mean fluorescence intensity was determined by flow cytometry (MFI; $n = 3$). **(D)** Histogram overlay profile generated from propidium iodide (PI) exclusion assay of cells treated as in **(A)**. **(E)** Graphical representation of MFI of PI-stained cells as in B; data presented is average mean fluorescence intensity (MFI) of 3 independent experiments.

analysis indicated that these genes were all interrelated, with the TNF-associated genes showing significant interrelationships (Figure 6A, red circles). In the STRING analysis, protein-coding genes *Lif, Birc3* and *Ccl2* were shown to be co-expressed while the products of genes *Fos, Mapk14, Birc3,* and *Fadd* have been experimentally determined to interact with each other.

In addition to the TNF-associated genes, several other genes were altered in the BMMC cultured on CNC/agarose and are worth noting (Figure 6B). Ten genes were downregulated or completely absent in the BMMC cultured on CNC/agarose. These genes included *Plec*, *Samd4b*, *Kmt2a*, *USP19*, *Herc2*, *Synj1*, *Zfp384-2*, *Traf3* and *Ints1*. *Synj1*, *Zfp384-2*, *Traf3* and *Ints1* which were almost completely absent in BMMC cultured on CNC/agarose. These genes were expressed by control BMMC cultured on agarose alone.

Seven genes were absent in the BMMC cultured on agarose alone, but upregulated in the BMMC cultured on CNC/agarose. These genes included heat shock proteins (*Hspa1b* and *Hspa1a*), transcription regulators (*Bclaf1*, *Pcnt*, *Zfp384-1* and *Ptbp3*) and a component of the TNF pathway (*Tnfrsf9*). Interestingly, culture of BMMC on CNC/agarose switched expression of Zfp384 transcripts from *Zfp384-2* to *Zfp384-1*.

To assess the potential contribution of transcription factors in the BMMC cytokine networks, we performed a search of transcription factors within our RNAseq transcript dataset using the *Mus musculus* database from the AnimalTFDB (Hu et al., 2019).

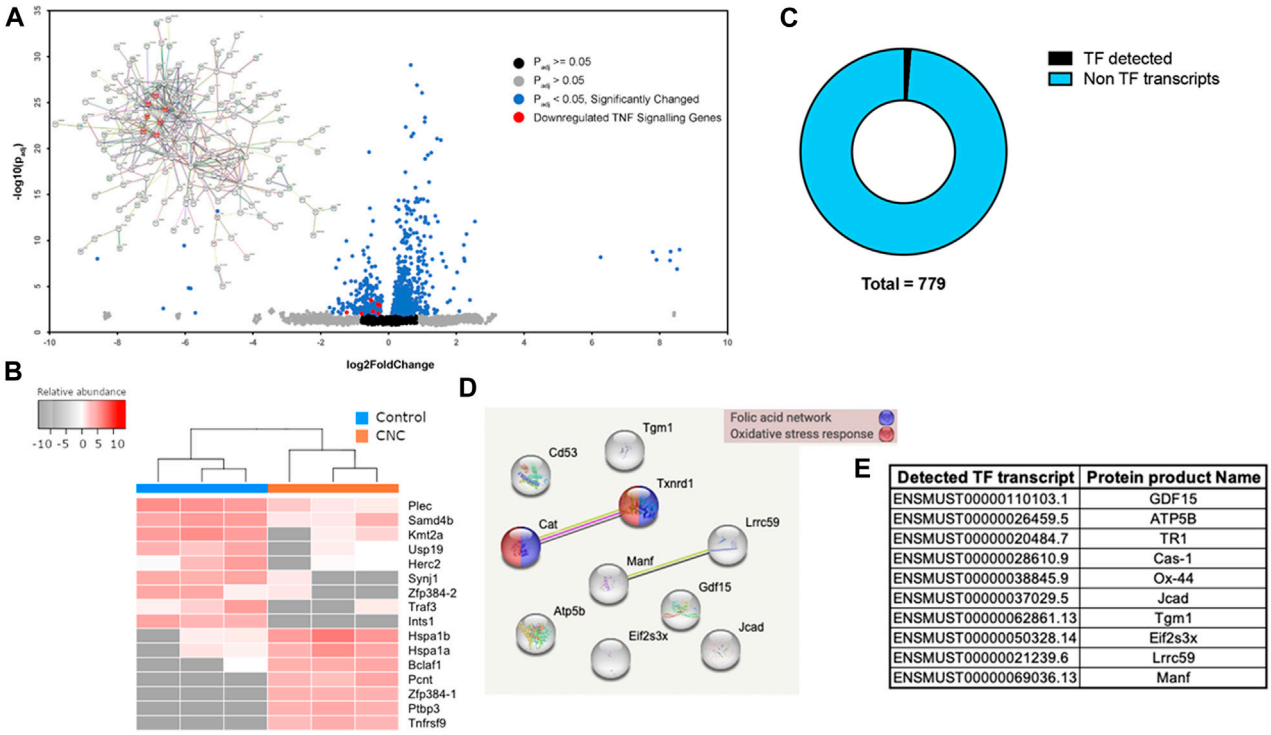

Detected TF transcript	Protein product Name
ENSMUST00000110103.1	GDF15
ENSMUST00000026459.5	ATP5B
ENSMUST00000020484.7	TR1
ENSMUST00000028610.9	Cas-1
ENSMUST00000038845.9	Ox-44
ENSMUST00000037029.5	Jcad
ENSMUST00000062861.13	Tgm1
ENSMUST00000050328.14	Eif2s3x
ENSMUST00000021239.6	Lrrc59
ENSMUST00000069036.13	Manf

FIGURE 6
RNASeq Analysts of gene expression of BMMC grown on 12.5% CNC/agarose. **(A)** Volcano plot and (inset) STRING analysis on downregulated genes. Genes related to TNF signaling pathway highlighted in red. **(B)** Top downregulated and upregulated transcripts in CNC samples as compared to control samples. Prior to plotting, data was subjected to a regularized logarithmic transformation that also corrects for sample size. Two transcripts of gene zinc finger protein 384 (Zfp384) were found deregulated, Zfp384-1 (ENSMUST00000112427) was found upregulated with a fold change of 320, while 4384-2 (ENSMUST00000112428) was found deregulated with a fold change of 52. (1 and 2 are arbitrary suffixes added to differentiate corresponding transcripts and are not part of the HGNC ID of the gene.) **(C)** ?Fs detected in RNAseq data set. Ten lfs were detected out of a total of 779 transcripts in the RNAseq dataset. **(D)** A STRING analysis suggests that TFs Cat (Cas-1, catalase) and Tx IMI (TRI, Thioredoxin reductase **(I)** are linked to folk acid network and oxidative stress response. **(E)** Ensembl ID for identified TF transcripts and protein names are shown.

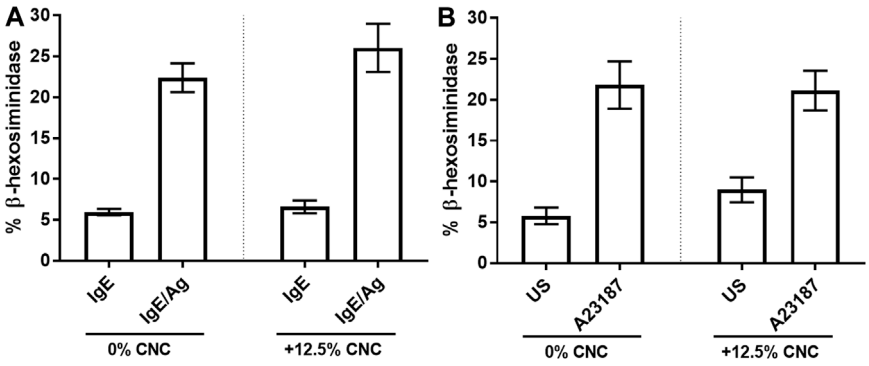

FIGURE 7
13-hexosaminidase release of BMMCs post incubation on CNC/agarose substrates. BMMC were cultured either in the absence (0% CNC) or presence (+12.5% CNC) of CNC/agarose substrates for 18 1.1, the cells were removed and activated with IgE and antigen (Ag) and 13-hexosaminidase release was measured. Cells sensitized with IgE alone (IgE) were used as a control. **(B)** BMMC were cultured as in **(A)** and activated with A23187 and 13-hexosaminidase release was measured. Uustimulated cells (US) were used as a control. Statistical analysis was performed using One-Way ANOVA with Tukey post-hoc test relative to activated cells incubated in the absence of CNC (0% CNC). Experiments were performed in quadruplicate with biological replicate of $n = 3$.

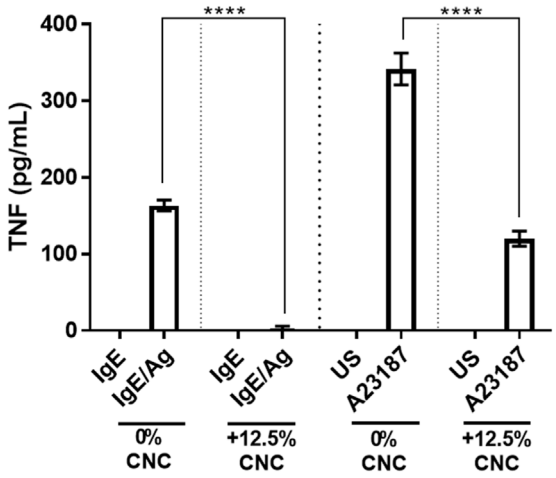

FIGURE 8
CNC/agarose matrix effect on BMMC mediator release. (A) BMMC were cultured in the absence (0)% CNC) or presence (12.5% CNC) of CNC/agarose substrates for 18 h, removed and activated with either IgE and antigen (Ag) where cells sensitized with IgE alone (IgE) were used as a control, or A23187 where unstimulated cells (US) were used as a control and their production of TNF was measured by ELISA. Statistical analysis was performed using One-Way ANOVA with Tukey post-hoc test relative to activated cells incubated in the absence of CNC (0% CNC), $p < 0.0001$ (****). Experiments were performed in triplicate with biological replicate of n-3.

From a total of 779 transcripts, 10 were identified as transcription factors (Figure 6C). A STRING analysis identified that 2 of these factors were involved in the folic acid network and oxidative stress response (Figure 6D). A table with the Ensembl ID and transcription factor protein names is shown in Figure 6E.

The CNC/agarose matrix does not modify BMMC degranulation in response to IgE-dependent and IgE-independent stimuli

One of the most critical requirements of a suitable 3D cell culture matrix is its ability to maintain normal cell function, particularly when cells are activated with stimuli. BMMC cultured on CNC/agarose or agarose alone were activated with IgE and antigen (IgE/Ag) which crosslinks their surface FcεRI receptors and initiates a series of signaling events leading to degranulation and mediator release. Although CNC/agarose appeared to increase the degranulation response of the BMMC when compared to BMMC cultured on agarose alone, this effect was not statistically significant (Figure 7A).

Next, BMMC that had been cultured on CNC/agarose or agarose alone were stimulated with A23187, a calcium ionophore which increases intracellular calcium concentration and initiates degranulation and the release of mediators stored in granules, including the lysosomal enzyme β-hexosaminidase. Degranulation of BMMC in response to A23187 did not change when the BMMC were cultured on agarose or CNC/agarose (Figure 7B). These results suggest that degranulation and the release of stored mediators is not affected by culture on the CNC/agarose hydrogel.

The CNC/agarose matrix inhibits BMMC production of cytokines, chemokines and other mediators when activated with IgE-dependent and IgE-independent stimuli.

BMMC cultured on CNC/agarose matrix were stimulated with IgE and antigen (IgE/Ag) which crosslinks their surface FcεRI receptors and also initiates a series of signaling events leading to the gene transcription and protein production of several pro-inflammatory mediators. Electrochemiluminescent multiplex screen analysis of several mediators indic7ated that BMMC activated with IgE/Ag produced IL-6 and MCP-1/CCL2 but not IL-4, IL-13, MMP-9 or RANTES (Supplementary Figures S2A–G). IgE/Ag-induced production of IL-5 and MCP-1/CCL2 was greatly reduced in BMMC that had been cultured on CNC/agarose, with almost complete absence of these cytokines in CNC/agarose-cultured BMMC (Supplementary Figures S2C, E). Interestingly, BMMC stimulated with A23187 produced IL-1β, IL-4, IL-6, IL-13, MCP-1/CCL2, MMP-9 and RANTES. However, BMMC cultured on CNC produced notably lower amounts of all of these mediators, especially IL-4, IL-13, MMP-9 and RANTES which were almost completely absent in CNC/agarose cultured BMMC (Supplementary Figures S2B, D, F, G). This data suggests that CNC has a profound inhibitory effect on production of these mediators by BMMC.

BMMC produce a significant amount of TNF that was not analyzed in the electrochemiluminescent multiplex analysis. To test for TNF production, BMMC were cultured and stimulated as described above, and TNF production was analyzed using ELISA. BMMC cultured on CNC/agarose released significantly less TNF when activated with IgE/Ag compared to BMMC cultured on agarose alone and activated with IgE/Ag (Figure 8). Similarly, BMMC cultured on CNC/agarose produced less TNF when activated with A23187 compared to BMMC cultured on agarose alone (Figure 8).

Discussion

Culture of cells on semi-solid media has been used to alter cell phenotype and allow for better manipulation of cells during culture. Although nanocellulose and its various forms have been used in many commercial products, the material's effects on cell culture and specifically cell phenotype, genotype and function are still poorly understood (Endes et al., 2016). Our analysis compared the culture of BMMC on agarose and CNC/agarose to better understand the influence of CNC on BMMC phenotype and function. Our analysis indicated that culture of BMMC on CNC/agarose leads to retention of FcεRI and KIT/CD117 expression and maintenance of membrane integrity, but a reduction in metabolic activity, altered gene expression and reduced mediator production upon activation with A23187 and IgE/Ag. These data suggest that culture with CNC is changing BMMC function without altering their phenotype and highlights the importance of semi-solid media composition on generating physiological cellular phenotypes.

EM analysis of the CNC/agarose matrix suggests that the gel forms a porous and complex structure, and that the addition of CNC significantly alters the morphology of the gel, creating ball-like structures that possibly contain liquid. This porous structure

would allow for the diffusion of nutrients and gases, perhaps providing a more amenable microenvironment for the cells. Although the cells were placed on top of this matrix, they likely experience slight changes in nutrient and waste product concentrations as they diffuse into the matrix below them. This may explain why the BMMC showed a general lack of change in viability and membrane integrity (Figure 3), suggesting that the cells were healthy overall and did not experience any adverse effects while cultured on CNC/agarose. Although there was a slight decrease in metabolic activity, this could be due to slight nutrient changes at the surface of the CNC/agarose gel. This could also be due to changes in oxygen levels leading to oxidative stress which can influence mitochondrial function. There are very few studies that have examined the effect of nanocellulose on oxidative stress, but some *in vivo* research has suggested that various forms of nanocellulose and cellulose nanocrystal-derived nano-onions can induce a slight increase in reactive oxygen species (ROS) generation in gut epithelium (DeLoid et al., 2019), and modulate oxidative stress in HEK293 cells (Abidi et al., 2021). Cationic derivatives of crystalline crystalline nanocellulose have induced mitochondrial ROS and ATP release in a mouse macrophage cell line (J774A1) and peripheral blood mononuclear cells (Sunasee et al., 2015). Both fibrillar and crystalline nanocellulose induce ROS generation (Wang et al., 2019). Nanocellulose fibrils have a more deleterious effect on oxidative stress in A549 lung epithelial cells compared to CNC, especially when CNC are incorporated into a gel (Menas et al., 2017). Wistar rats treated with nanocellulose showed an elevation in biomarkers associated with renal oxidative damage and increased expression of inducible nitric oxide synthase and COX-2, suggesting inflammation (Adewuyi et al., 2018). Yet, it remains to be determined whether CNC can directly affect NADPH generation in BMMC.

One surprising observation was that although BMMC cultured on CNC/agarose were able to degranulate normally (Figure 7), when activated with either A23187 or IgE/Ag, they produced significantly less *de novo* synthesized mediators that require transcription and translation (Figure 8). This decrease in mediator-producing capacity appeared to be reasonably universal such that the production of every mediator that was measured was significantly reduced. This is in contrast to A549 epithelial cells that increase cytokine and chemokine production when exposed to CNC—increasing their production of IL-6, IL-8, MCP-1, IL-1β, IL-12p70 and G-CSF after 72 h of exposure (Menas et al., 2017). In fact, several inflammatory mediators were produced by A549 cells, suggesting a general upregulation of several transcription pathways in these cells (Menas et al., 2017). In contrast, our RNAseq analysis indicated that there was a more balanced response to CNC by BMMC—with some genes upregulated, but others downregulated, suggesting that BMMC were choosing specific responses to their new microenvironment, rather than reacting ad-hoc.

BMMC cultured on CNC/agarose upregulated 7 genes that were effectively absent in cells that were cultured on agarose alone. These genes include heat shock proteins *Hspa1a* and *Hspa1b* which serve as chaperones for other proteins involved in cytoskeleton function and have been associated with atrial fibrillation and colorectal polyp formation (Szczuka et al., 2021; van Marion et al., 2021). These proteins appear to be essential in cellular responses to changes in microenvironment and therefore it is unsurprising that their expression is induced in BMMC cultured on CNC/agarose. *Bclaf1*, another gene that was upregulated in BMMC cultured on CNC/agarose as compared to control, is a transcription factor regulator that has a wide range of biological functions, including extracellular vesicle production and DNA damage responses (Jin et al., 2022). The role of *Bclaf1* in BMMC function and gene transcription has not been explored but it is likely that it is mediating some overall changes in cell phenotype.

BMMC cultured on CNC/agarose also upregulated several transcription regulators and regulators of cell division (*Pcnt*, *Zfp384-1* and *Ptbp3*). *Pcnt* encodes pericentrin, a protein found in centrosomes which regulate the assembly of microtubules during cell division. Pericentrin function in mast cells or the effect of CNC on its expression is unknown. However, pericentrin is an essential protein in spindle formation and cell cycle progression of cells (Chinen et al., 2021) and thus may be an important component of BMMC cell division in this new microenvironment.

Ptbp3 encodes a protein that is critical in RNA splicing and transcriptional regulation (Xie et al., 2022). The PTBP3 protein mediates TGF-β-induced epithelial-to-mesenchymal transition (Dong et al., 2022) and can serve as an immunomodulatory biomarker of cancer (Chen et al., 2022). Its expression and function in mast cells is unknown.

Interestingly, culture of BMMC switched expression of the zinc finger transcription factor *Zfp384* from the *Zfp384-2* to the *Zfp384-1* isoform, suggesting that the different isoforms have opposite functions in these two microenvironments. To our knowledge this type of switch in expression has not been described before. ZFP384 is also known as nuclear matrix protein 4 (NMP4) and was originally identified as a parathyroid hormone-responsive nuclear matrix architectural transcription factor that regulates gene activity by bending DNA (Torrungruang et al., 2002; Childress et al., 2015; Rump et al., 2016). Recent work has shown that ZFP384/NMP4 may directly bind IL-1β (Nakamoto et al., 2016) and bind to the promoter and/or non-coding sequences of chemokines CCL2, CCL7 and CXCL1 in lung epithelial cells and bone marrow-derived macrophages (Yang et al., 2021).

BMMC cultured on CNC/agarose also upregulated a component of the TNF pathway, TNF receptor superfamily member 9 (*Tnfrsf9*). TNFRSF9 is an important regulator of mast cell function in several pathologies, including Lewis lung carcinoma in mouse models (Wensman et al., 2012), and TNF production and signaling in mast cells has been recognized as an important aspect of their function for decades. To follow up on this observation, TNF production by BMMC cultured on CNC/agarose was determined. As with most of the mediators tested, BMMC cultured on CNC/agarose produced less TNF than BMMC cultured on agarose, suggesting that CNC/agarose modified the TNF pathways in complex ways—upregulating some components while downregulating others. Interestingly, this change in response did not affect degranulation, since BMMC cultured on CNC/agarose

degranulated similarly to BMMC cultured on agarose alone (Figure 7).

In conclusion, our data indicate that culture of BMMC on CNC/agarose leads to maintenance of mast cell integrity, degranulation and biomarker expression but inhibits their production of *de novo* synthesized mediators. This change in phenotype appears to be specific to newly synthesized mediators that require transcription and translation, suggesting that CNC/agarose modifies mast cells such that these pathways are fundamentally altered. Although the cells produced fewer mediators, their expression of mast cell receptors, CD117 and FcεRI were unaltered, demonstrating that the differentiation of these cells remain constant. Overall, our data suggest that CNC/agarose may be a viable option for the culture of BMMC in a 3D culture system, although their production of mediators may be altered.

Data availability statement

Raw sequencing data associated to this study is publicly available at the SRA database of NCBI under the accession number PRJNA938749.

Ethics statement

The animal tissues were obtained under approval from the Animal Ethics Committee at the University of Alberta (exemption ETR53).

Author contributions

AW and SBA generated the cell culture and cell function data. J-YC generated the cryo-SEM images. LK isolated RNA for the RNAseq analysis. JJ, JS, and MM-P generated and analyzed the RNAseq data. MK secured funding, obtained biosafety approvals, designed the experiments, analyzed the data, wrote the first draft of the manuscript and approved the final draft of the manuscript. All authors approved the final version of the figures and manuscript.

Funding

Funding was provided by the National Research Council Canada.

Acknowledgments

We thank Narcy Arizmendi for her technical assistance with the flow cytometry analysis of the BMMC. We thank Innotech Alberta for providing the CNC materials, and Ken Harris for proof-editing the manuscript.

Conflict of interest

The authors declare that the research was conducted in the absence of any commercial or financial relationships that could be construed as a potential conflict of interest.

Publisher's note

All claims expressed in this article are solely those of the authors and do not necessarily represent those of their affiliated organizations, or those of the publisher, the editors and the reviewers. Any product that may be evaluated in this article, or claim that may be made by its manufacturer, is not guaranteed or endorsed by the publisher.

Supplementary material

The Supplementary Material for this article can be found online at: https://www.frontiersin.org/articles/10.3389/fbioe.2023.1160460/full#supplementary-material

References

Abidi, S. M. S., Dar, A. I., and Acharya, A. (2021). Multifunctional gold nanoparticle-conjugated cellulose nanoonions alleviate Aβ42 fibrillation-induced toxicity via regulation of oxidative stress and ion homeostasis. *Biomacromolecules* 22 (6), 2419–2435. Epub 20210504. doi:10.1021/acs.biomac.1c00228

Adewuyi, A., Otuechere, C. A., Adebayo, O. L., Anazodo, C., and Pereira, F. V. (2018). Renal toxicological evaluations of sulphonated nanocellulose from khaya sengalensis seed in wistar rats. *Chem. Biol. Interact.* 284, 56–68. Epub 20180216. doi:10.1016/j.cbi.2018.02.015

Alam, S. B., Wagner, A., Willows, S., and Kulka, M. (2022). Quercetin and resveratrol differentially decrease expression of the high-affinity IgE receptor (FcεRI) by human and mouse mast cells. *Molecules* 27 (19), 6704. doi:10.3390/molecules27196704

Benassi, J. C., Barbosa, F. A. R., Candiotto, G., Grinevicius, V., Filho, D. W., Braga, A. L., et al. (2022). Docking and molecular dynamics predicted B-DNA and dihydropyrimidinone selenoesters interactions elucidating antiproliferative effects on breast adenocarcinoma cells. *J. Biomol. Struct. Dyn.* 40 (18), 8261–8273. doi:10.1080/07391102.2021.1910569

Bienenstock, J., Tomioka, M., Matsuda, H., Stead, R. H., Quinonez, G., Simon, G. T., et al. (1987). The role of mast cells in inflammatory processes: Evidence for nerve/mast cell interactions. *Int. Arch. Allergy Appl. Immunol.* 82 (3-4), 238–243. doi:10.1159/000234197

Biranje, S. S., Sun, J., Cheng, L., Cheng, Y., Shi, Y., Yu, S., et al. (2022). Development of cellulose nanofibril/casein-based 3d composite hemostasis scaffold for potential wound-healing application. *ACS Appl. Mater Interfaces* 14 (3), 3792–3808. doi:10.1021/acsami.1c21039

Bray, N. L., Pimentel, H., Melsted, P., and Pachter, L. (2016). Erratum: Near-Optimal probabilistic rna-seq quantification. *Nat. Biotechnol.* 34 (8), 888. doi:10.1038/nbt0816-888d

Bray, N. L., Pimentel, H., Melsted, P., and Pachter, L. (2016). Near-optimal probabilistic rna-seq quantification. *Nat. Biotechnol.* 34 (5), 525–527. doi:10.1038/nbt.3519

Chen, C., Shang, A., Gao, Y., Huang, J., Liu, G., Cho, W. C., et al. (2022). Ptbps: An immunomodulatory-related prognostic biomarker in pan-cancer. *Front. Mol. Biosci.* 9, 968458. Epub 20220823. doi:10.3389/fmolb.2022.968458

Childress, P., Stayrook, K. R., Alvarez, M. B., Wang, Z., Shao, Y., Hernandez-Buquer, S., et al. (2015). Genome-wide mapping and interrogation of the Nmp4 antianabolic bone Axis. *Mol. Endocrinol.* 29 (9), 1269–1285. Epub 20150805. doi:10.1210/me.2014-1406

Chinen, T., Yamazaki, K., Hashimoto, K., Fujii, K., Watanabe, K., Takeda, Y., et al. (2021). Centriole and pcm cooperatively recruit Cep192 to spindle Poles to promote bipolar spindle assembly. *J. Cell Biol.* 220 (2), e202006085. doi:10.1083/jcb.202006085

DeLoid, G. M., Cao, X., Molina, R. M., Silva, D. I., Bhattacharya, K., Ng, K. W., et al. (2019). Toxicological effects of ingested nanocellulose in *in vitro* intestinal epithelium and *in vivo* rat models. *Environ. Sci. Nano* 6 (7), 2105–2115. Epub 20190618. doi:10.1039/c9en00184k

Denburg, J. A., Richardson, M., Telizyn, S., and Bienenstock, J. (1983). Basophil/mast cell precursors in human peripheral blood. *Blood* 61 (4), 775–780. doi:10.1182/blood.v61.4.775.bloodjournal614775

Dong, C., Wu, K., Gu, S., Wang, W., Xie, S., and Zhou, Y. (2022). Ptbp3 mediates tgf-beta-induced emt and metastasis of lung adenocarcinoma. *Cell Cycle* 21 (13), 1406–1421. Epub 20220324. doi:10.1080/15384101.2022.2052530

Endes, C., Camarero-Espinosa, S., Mueller, S., Foster, E. J., Petri-Fink, A., Rothen-Rutishauser, B., et al. (2016). A critical review of the current knowledge regarding the biological impact of nanocellulose. *J. Nanobiotechnology* 14 (1), 78. Epub 20161201. doi:10.1186/s12951-016-0230-9

Gabr, S. A., Elsaed, W. M., Eladl, M. A., El-Sherbiny, M., Ebrahim, H. A., Asseri, S. M., et al. (2022). Curcumin modulates oxidative stress, fibrosis, and apoptosis in drug-resistant cancer cell lines. *Life (Basel)* 12 (9), 1427. Epub 20220913. doi:10.3390/life12091427

Hu, H., Miao, Y. R., Jia, L. H., Yu, Q. Y., Zhang, Q., and Guo, A. Y. (2019). Animaltfdb 3.0: A comprehensive resource for annotation and prediction of animal transcription factors. *Nucleic Acids Res.* 47 (D1), D33–D38. doi:10.1093/nar/gky822

Jin, Y., Anbarchian, T., and Nusse, R. (2022). Assessment of hepatocyte ploidy by flow cytometry. *Methods Mol. Biol.* 2544, 171–181. doi:10.1007/978-1-0716-2557-6_12

Karamchand, L., Wagner, A., Alam, S. B., and Kulka, M. (2021). Fabrication of a crystalline nanocellulose embedded agarose biomaterial ink for bone marrow-derived mast cell culture. *J. Vis. Exp.* 171. doi:10.3791/62519

Kurosawa, H. (2007). Methods for inducing embryoid body formation: *In vitro* differentiation system of embryonic stem cells. *J. Biosci. Bioeng.* 103 (5), 389–398. doi:10.1263/jbb.103.389

Love, M. I., Huber, W., and Anders, S. (2014). Moderated estimation of fold change and dispersion for rna-seq data with Deseq2. *Genome Biol.* 15 (12), 550. doi:10.1186/s13059-014-0550-8

Ma, N., Cheung, D. Y., and Butcher, J. T. (2022). Incorporating nanocrystalline cellulose into a multifunctional hydrogel for heart valve tissue engineering applications. *J. Biomed. Mater Res. A* 110 (1), 76–91. doi:10.1002/jbm.a.37267

Matsumura, T., Totani, H., Gunji, Y., Fukuda, M., Yokomori, R., Deng, J., et al. (2022). A myb enhancer-guided analysis of basophil and mast cell differentiation. *Nat. Commun.* 13 (1), 7064. Epub 20221118. doi:10.1038/s41467-022-34906-1

Menas, A. L., Yanamala, N., Farcas, M. T., Russo, M., Friend, S., Fournier, P. M., et al. (2017). Fibrillar vs crystalline nanocellulose pulmonary epithelial cell responses: Cytotoxicity or inflammation? *Chemosphere* 171, 671–680. Epub 20161224. doi:10.1016/j.chemosphere.2016.12.105

Moriyama, A., Ogura, I., and Fujita, K. (2022). Potential issues specific to cytotoxicity tests of cellulose nanofibrils. *J. Appl. Toxicol.* 43, 195–207. doi:10.1002/jat.4390

Mortensen, N. P., Moreno Caffaro, M., Davis, K., Aravamudhan, S., Sumner, S. J., and Fennell, T. R. (2022). Investigation of eight cellulose nanomaterials' impact on differentiated caco-2 monolayer integrity and cytotoxicity. *Food Chem. Toxicol.* 166, 113204. doi:10.1016/j.fct.2022.113204

Nakahata, T., Spicer, S. S., Cantey, J. R., and Ogawa, M. (1982). Clonal assay of mouse mast cell colonies in methylcellulose culture. *Blood* 60 (2), 352–361. doi:10.1182/blood.v60.2.352.bloodjournal602352

Nakamoto, T., Izu, Y., Kawasaki, M., Notomi, T., Hayata, T., Noda, M., et al. (2016). Mice deficient in ciz/nmp4 develop an attenuated form of K/Bxn-Serum induced arthritis. *J. Cell Biochem.* 117 (4), 970–977. Epub 20150930. doi:10.1002/jcb.25382

Ogawa, M., Suda, T., and Suda, J. (1984). Differentiation and proliferative kinetics of hemopoietic stem cells in culture. *Prog. Clin. Biol. Res.* 148, 35–43.

Pandanaboina, S. C., RanguMagar, A. B., Sharma, K. D., Chhetri, B. P., Parnell, C. M., Xie, J. Y., et al. (2021). Functionalized nanocellulose drives neural stem cells toward neuronal differentiation. *J. Funct. Biomater.* 12 (4), 64. doi:10.3390/jfb12040064

Rump, K., Siffert, W., Peters, J., and Adamzik, M. (2016). The transcription factor Nmp4 binds to the Aqp5 promoter and is a novel transcriptional regulator of the Aqp5 gene. *DNA Cell Biol.* 35 (7), 322–327. Epub 20160408. doi:10.1089/dna.2015.3110

Samarghandian, S., Azimi-Nezhad, M., and Farkhondeh, T. (2019). Thymoquinone-induced antitumor and apoptosis in human lung adenocarcinoma cells. *J. Cell Physiol.* 234 (7), 10421–10431. Epub 20181101. doi:10.1002/jcp.27710

Sunasee, R., Araoye, E., Pyram, D., Hemraz, U. D., Boluk, Y., and Ckless, K. (2015). Cellulose nanocrystal cationic derivative induces NLRP3 inflammasome-dependent IL-1β secretion associated with mitochondrial ROS production. *Biochem. Biophys. Rep.* 4, 1–9. Epub 20150814. doi:10.1016/j.bbrep.2015.08.008

Szczuka, I., Wierzbicki, J., Serek, P., Szczesniak-Siega, B. M., and Krzystek-Korpacka, M. (2021). Heat shock proteins Hspa1 and Hsp90aa1 are upregulated in colorectal polyps and can Be targeted in cancer cells by anti-inflammatory oxicams with arylpiperazine pharmacophore and benzoyl moiety substitutions at thiazine ring. *Biomolecules* 11 (11), 1588. Epub 20211027. doi:10.3390/biom11111588

Torrungruang, K., Alvarez, M., Shah, R., Onyia, J. E., Rhodes, S. J., and Bidwell, J. P. (2002). DNA binding and gene activation properties of the Nmp4 nuclear matrix transcription factors. *J. Biol. Chem.* 277 (18), 16153–16159. Epub 20020226. doi:10.1074/jbc.M107496200

Ugrin, M., Dinic, J., Jeremic, S., Dragicevic, S., Banovic Djeri, B., and Nikolic, A. (2021). Bacterial nanocellulose as a scaffold for *in vitro* cell migration assay. *Nanomater. (Basel)* 11 (9), 2322. doi:10.3390/nano11092322

van Marion, D. M. S., Ramos, K. S., Lanters, E. A. H., Bulte, L. B., Bogers, A., de Groot, N. M. S., et al. (2021). Atrial heat shock protein levels are associated with early postoperative and persistence of atrial fibrillation. *Heart* 18 (10), 1790–1798. Epub 20210626. doi:10.1016/j.hrthm.2021.06.1194

Wang, X., Chang, C. H., Jiang, J., Liu, Q., Liao, Y. P., Lu, J., et al. (2019). The crystallinity and aspect ratio of cellulose nanomaterials determine their pro-inflammatory and immune adjuvant effects *in vitro* and *in vivo*. *Small* 15 (42), e1901642. Epub 20190828. doi:10.1002/smll.201901642

Wensman, H., Kamgari, N., Johansson, A., Grujic, M., Calounova, G., Lundequist, A., et al. (2012). Tumor-mast cell interactions: Induction of pro-tumorigenic genes and anti-tumorigenic 4-1bb in mcs in response to Lewis lung carcinoma. *Mol. Immunol.* 50 (4), 210–219. Epub 20120218. doi:10.1016/j.molimm.2012.01.009

Xie, C., Long, F., Li, L., Li, X., Ma, M., Lu, Z., et al. (2022). Ptbp3 modulates P53 expression and promotes colorectal cancer cell proliferation by maintaining Ube4a mrna stability. *Cell Death Dis.* 13 (2), 128. Epub 20220208. doi:10.1038/s41419-022-04564-8

Yang, S., Adaway, M., Du, J., Huang, S., Sun, J., Bidwell, J. P., et al. (2021). Nmp4 regulates the innate immune response to influenza a virus infection. *Mucosal Immunol.* 14 (1), 209–218. Epub 20200309. doi:10.1038/s41385-020-0280-z